

Effects of the Thickness of Boundary Layer on Droplet's Evaporation Rate

P. Jonglearttrakull and K. Fushinobu

School of Engineering, Department of Mechanical Engineering, Tokyo Institute of Technology, 2-12-1 Ookayama, Meguro City, Tokyo 152-8550, Japan

E-mail: jonglearttrakull.p.aa@m.titech.ac.jp

M. Kadonaga

Integrated Product Strategy Planning Section, Business Strategy Department, Ricoh Company, Ltd., 1- 3-6, Nakamagome, Ohta-ku, Tokyo 143-8555, Japan

School of Engineering, Department of Mechanical Engineering, Tokyo Institute of Technology, 2-12-1 Ookayama, Meguro City, Tokyo 152-8550, Japan

Abstract. *The evaporation rate of a droplet was explained in relation to the thickness of the boundary layer and the condition near the droplet's surface. However, the number of results obtained from experiments is very limited. This study aims to investigate the thickness of the boundary layer of an ethanol–water mixture droplet and its effect on the evaporation rate by Z-type Schlieren visualization. Single and double droplets are tested and compared to identify the effect of the second droplet on the average and instantaneous evaporation rate. The double droplet's lifetime is found to be longer than the single droplet's lifetime. The formation of a larger vapor region on the top of the droplet indicates a higher instantaneous evaporation rate. The thickness of the boundary layer is found to increase with increase in ethanol concentration. Furthermore, a larger vapor distribution area is found in the case of higher ethanol concentration, which explains the faster evaporation rate at higher ethanol concentration. © 2020 Society for Imaging Science and Technology.*

[DOI: 10.2352/J.ImagingSci.Technol.2020.64.5.050402]

1. INTRODUCTION

The evaporation of sessile droplets has been applied in many engineering applications such as inkjet printing [1–7], coating technology [8, 9], and DNA stretching and deposition [10–13]. This process is usually observed in daily life phenomena such as drying water and rain drops. As regards the printing industry, inkjet printers have been widely used due to their many advantages: low-cost printing, accuracy, and a high printing rate. Although its market is growing very fast, problems related to print quality have emerged recently. During series of paper printing, drops of ink are sometimes not completely evaporated. Incompletely evaporated ink may cause the following problems: penetration of unevaporated ink into the upper paper in the printer's tray or unintentional touching of unevaporated ink by humans. In addition, the print quality is degraded. Consequently, the study of

ink evaporation is required to reduce the effect of the above-mentioned problems.

Evaporation models of droplets have been studied by many researchers. Lebedev et al. [14] employed the similarity between diffusion fields and electrostatic fields to derive an evaporation equation for spherical droplets. Picknett and Bexon [15] studied the evaporation of sessile droplets in still air by which stages of evaporation were first defined. These were in contact angle and contact line area states. Their results motivated other researchers to deeply investigate the behavior of droplets with various properties. Birdi et al. [16] calculated the evaporation rate of a droplet by using the rate of diffusion of vapor. Deegan et al. [17, 18] used the Laplace equation to solve the hemispherical droplet model, which was simpler than the previous models. Later, Hu et al. [19] experimentally investigated the sessile droplet with a pinned contact line by a theoretical method and the finite element method and found an expression that related evaporation rate to the contact angle and the radius of the droplet. Semenov et al. [20] studied the behaviors of the droplet's contact angle and radius. Three stages of evaporation were found including a short spreading stage in which evaporation can be neglected; this stage continues until the contact angle reaches an advancing contact angle and the radius becomes maximum. In stage 1, the first stage of evaporation begins, and it is characterized by a constant radius, where the contact angle reduces from an advancing contact angle to a receding contact angle. In stage 2, evaporation continues at a constant contact angle and a reduction in the droplet radius. Stage 3 is the final evaporation stage, where both the contact angle and the radius decrease until the droplet completely evaporates. However, the experiments from the literature mentioned above were generally performed by using a camera and a liquid droplet. Nonetheless, other measurement techniques, adjustments, and conditions were also applied to investigate the physics of the liquid droplet. For example, Girard et al. [21, 22] employed infrared (IR) thermography to measure the temperature profile of a water

Received Apr. 5, 2020; accepted for publication July 26, 2020; published online Aug. 24, 2020. Associate Editor: Jihoon Kim.

1062-3701/2020/64(5)/050402/11/\$25.00

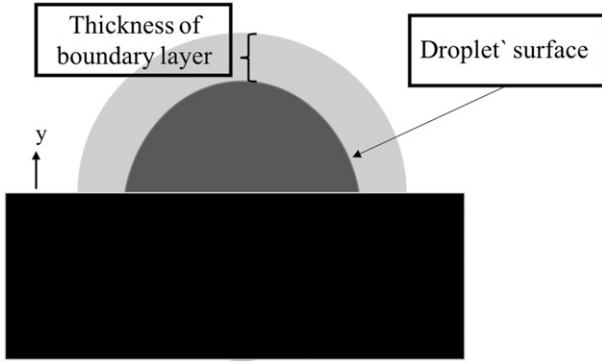


Figure 1. The thickness of boundary layer on the surface of a droplet.

droplet on a heated substrate and found that the time evolution of the local evaporative mass flux was constant at the apex of the droplet but increased near the contact line. Moreover, since the contact line could be observed from the interfacial temperature profile, this created the possibility of investigating the dynamics of the contact line during the sudden decrease in contact angle during evaporation.

The aforementioned literature reviews [14–20] show that evaporation rate models of droplets can be categorized into the spherical droplet model, in which the evaporation rate relates to both the contact angle and the radius, and the hemispherical droplet model, in which the evaporation rate relates only to the radius of the droplet. However, these models were derived with the assumption that the length of the diffusion layer or the field of vapor over the droplet was very large compared to the radius of the droplet, which was approximately $20R$ as mentioned by Hu et al. [19]. The evaporation of the droplet from another point of view was introduced by Yamaue [23]. An equation of droplet evaporation was presented in terms of the diffusion layer of the solvent vapor formed on the surface of the droplet not approaching infinity but measurable as shown in the following equation:

$$J(R) = D_{\text{gas}} (C_v - C_a) \left(\frac{1}{R} + \frac{1}{l} \right), \quad (1)$$

where $J(R)$ [m/s] is the evaporation rate, D_{gas} [m²/s] is the diffusion coefficient of the gas phase, C_v is the vapor concentration (volume fraction) on the droplet's surface, C_a is the vapor concentration (volume fraction) in the atmosphere, R [m] is the radius of the droplet, and l [m] is the thickness of the diffusion layer.

In this study, the thickness of the diffusion layer is defined as the droplet's boundary layer thickness, and Figure 1 shows the schematics. However, the thickness of the boundary layer has been obtained only from simulation, and few experiments to measure the thickness of the boundary layer value have been conducted. Kobayashi et al. [24] and Doi [25] studied the condition near the water droplet's surface and reported that if there is another water droplet B near water droplet A, the water vapor pressure around A will increase and that the increase in the vapor pressure suppresses the average evaporation rate. In addition, average

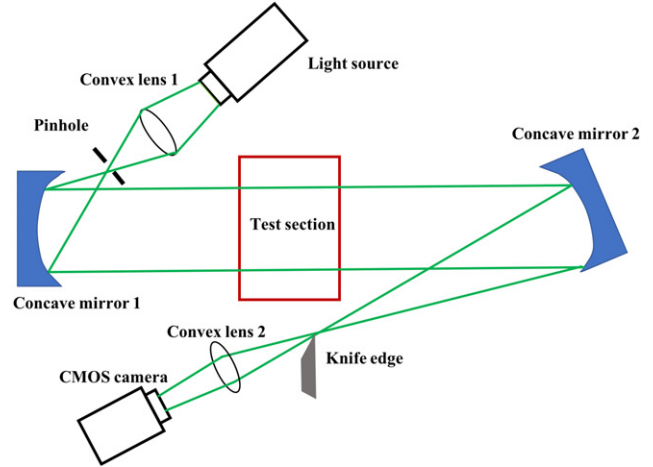


Figure 2. Schematic of the Z-type Schlieren setup.

evaporation per droplet in the double droplet case was presented as the following equation:

$$\bar{J}(L) = \frac{\bar{J}(\infty)}{1 + R/L}, \quad (2)$$

where $\bar{J}(L)$ [m/s] is the average evaporation rate per droplet in the double droplet case, L [m] is the distance between the centers of both droplets, $\bar{J}(\infty)$ [m/s] is the evaporation rate of a single droplet (when $L \rightarrow \infty$), and R [m] is the droplet radius.

Schlieren visualization has been used for several decades. It is a convenient technique to monitor and identify fluid properties that normally relate to refractive index values such as density, temperature, and concentration. Hence, it can be used to identify and measure a droplet's boundary layer thickness from the difference of refractive indexes between vapor and the surrounding air. Among several types of Schlieren techniques, Z-type Schlieren is one of the most widely utilized methods due to its many advantages such as high sensitivity, simple setting, and low construction cost.

The schematic diagram of Z-type Schlieren is presented in Figure 2. Light rays, which orthogonally travel through changes in refractive index fields, deflect and bend toward the higher refractive index regions while undisturbed rays continue traveling in the same direction as the initial direction. Reflected light rays are partially blocked by the knife edge, forming darkened and brightened regions, which are detected by a camera. Because of this reflection, the refractive angle can be expressed in relation to the refractive index as in the following equation:

$$\varepsilon_y = \frac{1}{n_{\text{air}}} \int \frac{\partial n}{\partial y} dz, \quad (3)$$

where ε_y is the refractive angle in the vertical direction, n_{air} is the air refractive index, which is assumed to be 1, n is the refractive index value at the coordinates y and z in the y - z plane, and z axis represents the direction of the light ray.

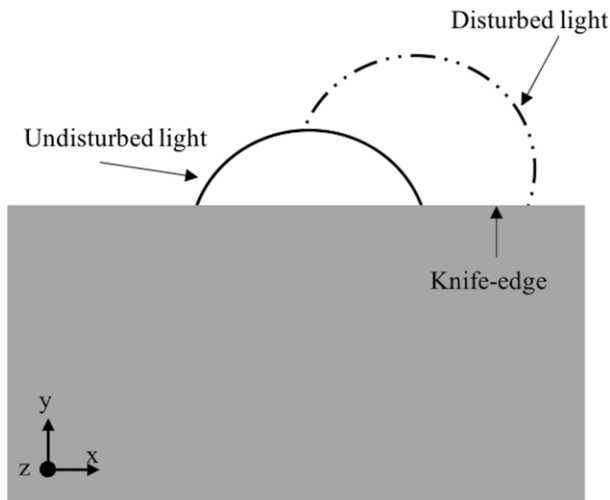


Figure 3. Knife-edge plane's diagram.

As described previously, both darkened and brightened regions are formed by the blocking of light at the knife edge. This can be simply described by the knife-edge plane's diagram as shown in Figure 3. By assuming a circular beam shape and that it is cut by a single-blade knife edge, the solid line represents undisturbed light while the dashed line represents disturbed light. Depending on the refractive index change in the test region, the deflected light at the knife-edge plane shifts to either a higher or a lower position compared to undisturbed light. In the case of higher shifting, a brighter image is obtained. Conversely, a darker image is identified in the case of lower shifting.

The measurement of droplets by the Schlieren system was reported by Kelly et al. [26]. However, only pure hydrocarbon liquids were used in their study. Hence, an ethanol–water mixture was selected instead of water-based ink because the sensitivity of the Schlieren system directly relates to the refractive index of the substance, and ethanol vapor ($n = 1.0008$ at 296K) has a higher refractive index than that of water vapor ($n = 1.00025$ at 296K).

Sefiane et al. [27] investigated the effect of ethanol concentration on the evaporation of a water–ethanol mixture on a rough polytetrafluoroethylene (PTFE) substrate. The following results were observed: the droplet's lifetime decreased as the ethanol concentration was increased, and a high ethanol concentration (75%) tended to follow the behavior of pure ethanol in the beginning and pure water at the end due to the difference in their volatile properties. Christy et al. [28] used particle image velocimetry to evaluate the flow field of the ethanol–water mixture to explain the states found by Sefiane et al. [27]. Liu et al. [29] conducted a study and reported that the ethanol fraction did not completely evaporate in the first stage, but it remained until the end of the evaporation period. Later, Shi et al. [30] studied the wettability of a binary mixture on a polished PTFE substrate and found the stick–slip behavior of the droplet, which showed consistency with the result by Sefiane et al. [27]. Cheng et al. [31] investigated the evaporation of an ethanol–water droplet

on a gold surface and identified three modes, which were pinning, evaporating, and shrinking. However, since the above-mentioned studies about ethanol–water evaporation were conducted on a non-heated substrate, Gurralla et al. [32] performed an experiment to evaluate the evaporation of an ethanol–water sessile droplet at different compositions and substrate temperatures. It was found that the lifetime of ethanol decreased as the temperature of the substrate increased as expected. Moreover, natural convection as well as additional terms due to the heated substrate were considered together with the diffusion term to create a more accurate model of the evaporation of a droplet. Recently, Katre et al. [33] introduced IR thermography to measure the dynamics inside an ethanol–water droplet on an inclined heated substrate. A water-rich cold region was observed around the advancing angle, which was observed to be pinned. On the other hand, a hotter region of ethanol was found around the receding angle, which rapidly decreased over time. Also, three distinct stages of contact line dynamics were found; stage 1, increasing of the advancing and receding angle; stage 2, slow decreasing of droplet contact angles; stage 3, both advancing and receding angle rapidly decrease. They also noticed that by imposing more conditions, such as an inclined or heated substrate, the dynamics of the ethanol–water sessile droplet became more complex.

As mentioned above, it is important to measure the boundary layer thickness of the ethanol–water mixture droplet to gain more understanding about its effect on the evaporation rate of the droplet and to experimentally estimate the thickness of the boundary layer.

The objectives of our study are to experimentally obtain the droplet's boundary layer thickness to interpret the difference in results between an ethanol–water mixture and pure substances and to find the effect on the evaporation rate if the neighboring second droplet exists. Moreover, since this study is the first time that we attempt to experimentally measure the droplet's boundary layer thickness, we will discuss about them by comparing and interpreting our result's trend and behaviors with the theory provided by the previous studies.

2. NUMERICAL CALCULATION

2.1 Refractive Angle and Shifted Light at the Knife Edge

The refractive angle originating from the deflection of light rays in the test region leads to the light shifting at the knife-edge plane. Referring to [34, 35], a relation between them can be expressed as the following equation:

$$\varepsilon_y = \frac{\Delta a}{f_2}, \quad (4)$$

where ε_y is the refractive angle in the vertical direction, Δa is the light shifting distance at the knife-edge plane, and f_2 is the focal length of the second concave mirror.

2.2 Knife-edge Position and Intensity

The knife-edge position strongly influences the light intensity captured by the camera. It is known as “percent

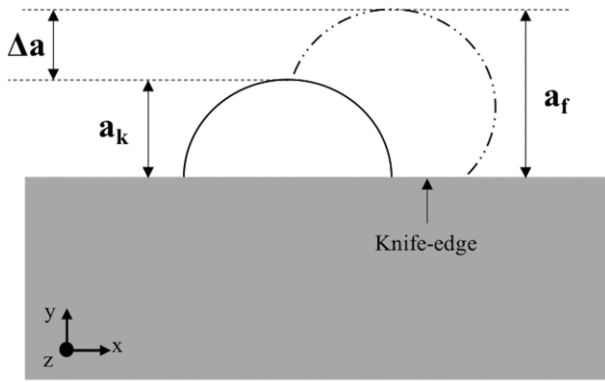


Figure 4. Schematics of light shifting distance at the knife edge.

cut-off.” The greater the cut-off percentage, the darker the image that is obtained. For calculating the refractive index value, the relation between them needs to be identified. Hernandez et al. [36] recorded the Schlieren image and created a calibration curve between the knife-edge position and the light intensity. By averaging all pixel intensity values in the image, the average value at each knife-edge position was subtracted by the average value of the reference image taken when the knife edge was placed at the reference position, i.e. when 40% of the intensity at the non-cut-off position was detected. A wide range of linear relations were roughly identified. Hence, the relation between the knife-edge position and the intensity is approximated as a linear relation in this study as expressed in the following equation:

$$I \propto a, \quad (5)$$

where I is the intensity of light captured by the camera and a represents the knife-edge vertical position.

The light shifting distance is defined by the difference in heights of light passing through the knife edge between undisturbed and disturbed light as shown in Figure 4. In addition, undisturbed light represents light without a change in the refractive index, i.e. no droplet or reference image, while disturbed light represents light passing through the area with the vapor formed on the droplet, i.e. the Schlieren image. The light shifting distance (Δa) is expressed as follows:

$$\Delta a = a_f - a_k, \quad (6)$$

where Δa is the light shifting distance, a_f is the height of light passing through the knife edge in the case of Schlieren image, and a_k is the value for the reference image, which is set to be 0.5 mm in this study.

Referring to the linear relation between the knife-edge position and the light intensity in Eq. (5), the relation between disturbed and undisturbed light intensities can be expressed as follows:

$$\frac{\Delta I}{I_k} = \frac{I_f - I_k}{I_k} = \frac{\Delta a}{a_k} = \frac{a_f - a_k}{a_k}, \quad (7)$$

where I_f represents the light intensity of the Schlieren image, I_k is the light intensity of the reference image, and ΔI is defined as $\Delta I = I_f - I_k$.

Normally, I is a function of x and y . Nevertheless, since the knife edge is placed in the horizontal direction, only a change in the perpendicular direction of the knife edge can be detected. Hence, $I(x, y)$ is reduced to $I(y)$. Consequently, $\Delta I(y)$ is obtained. In this calculation, $\Delta I(y)$ is fitted by a second-order polynomial due to a lower calculation time.

2.3 Refractive Index Equation

By combining Eqs. (3), (4), and (7), the following equation is obtained:

$$\int \frac{\partial n}{\partial y} dz = \left(\frac{\Delta I(y)}{I_k} \right) \left(\frac{a_k}{f_2} \right). \quad (8)$$

Assuming that the refractive index is independent of z and $\int dz$ approximately equals the diameter of the droplet in the beginning, Eq. (8) is reduced to the following equation:

$$\frac{\partial n}{\partial y} = \left(\frac{1}{d_i} \right) \left(\frac{\Delta I(y)}{I_k} \right) \left(\frac{a_k}{f_2} \right), \quad (9)$$

where d_i is the droplet's initial diameter.

3. METHODS

3.1 The Z-type Schlieren Setup

The experimental system was constructed by using optical equipment. According to the size of the droplet, a small optical equipment was used. White light originating from an LED light source (Luminar Ace LA-HDF108A 20 W) was passed through the first convex lens with a focal length of 100 mm and a diameter of 20 mm. A pinhole with a diameter of 500 μ m was placed at the focal point of the first convex lens and the first concave mirror (spherical mirror, f300, \varnothing 20 mm) to create a point light source. The first concave mirror was installed and used to parallel the light since the diameter of light leaving the pinhole increased while traveling along the z axis. In other words, the light rays became parallel and the diameter of the beam became constant after the reflection at the first concave mirror. The PTFE substrate was placed at the test section located between the first and second concave mirrors. Parallel light rays were focused at the focal point of the second concave mirror (spherical mirror, f1000, \varnothing 20 mm) at which the single-blade knife edge was placed. The second convex lens was installed before the CMOS camera (Allied Vision Mako G-234B 1/1.2” Monochrome CMOS Camera, 1936 \times 1216 pixels) to ensure that light passing through the knife edge would be perfectly focused on the camera.

3.2 Experimental Procedures

An ethanol–water mixture was used instead of water-based ink since the refractive index of water vapor is very close to that of air. Since Schlieren visualization utilizes the difference in refractive indexes to identify the vapor region, it would be more difficult to detect the vapor region if water-based ink is used. Ethanol–water mixtures were prepared at 100% (pure ethanol), 75%, 50%, 25%, and 0% (pure water) by volume

Table I. Ambient temperature (T_a) and relative humidity ratio (%RH) of each experiment for single droplet and double droplet.

Cases	100% et		75% et		50% et		25% et		0% et	
	T_a ($^{\circ}$ C)	%RH								
Single	25.1	26.1	26.2	32.4	27.4	30.1	25.8	27.9	24.7	30.7
Double	25.4	45.3	24.7	42.5	25.6	39.7	25.7	46.7	27.5	38.8

fraction. Three experiments were conducted in each case, and the average result was utilized to increase the confidence of the experimental result. Single and double droplet cases were tested, and their results were compared. In the double droplet case, both droplets were dropped at the same time, and the final result was obtained by averaging both droplets' results. Even though the actual volume of the droplet used for an inkjet printer is about 10–80 pL, a larger size of the droplet that could be monitored by the system was employed. Hence, a small droplet of 2.5 μ L was created by an Eppendorf micropipette. All experiments were performed at ambient temperatures of 24–28 $^{\circ}$ C and relative humidities of 25–50%; the ambient temperature and the relative humidity for each case are shown in Table I. Vimba together with MATLAB's image acquisition tool was used to obtain the results. In fact, frame capturing per second (fps) or the frame rate should be set as fast as possible since more images could be captured and thus more details could be obtained. However, in this study, it was set between 0.6 and 4 fps depending on the ethanol–water mixture concentration due to the limitation of computational capability. Before each experiment started, 200 snapshots of the image were captured at 4 fps and used as the reference picture. After the droplet was deposited, images were captured until it completely evaporated. The substrate was cleaned up each time by Kimwipe tissue, and the surrounding air was blown before a new experiment was started to confirm that there was no evaporation effect from the previous experiment.

3.3 Image Processing

To obtain ΔI , subtraction between Schlieren and reference images is required. In the following analysis, image (A) represents the reference image, which is the picture without the droplet as shown in Figure 5(a). Therefore, neither the droplet nor the evaporation effect was present in (A). On the other hand, image (B) represents the Schlieren image in which both droplet and evaporation effects were present as illustrated in Fig. 5(b). Hence, after subtraction between (A) and (B), image (C) was obtained in which the pure evaporation effect of the droplet was clearly identified and instantaneously differentiated from the surrounding air as shown in Fig. 5(c). Consequently, the difference in intensity (ΔI) was fitted at a vertical position to obtain $\Delta I(y)$. The intensity of the reference image I_k and subsequently the refractive index field were directly determined from Eq. (9). According to the described calculation processes, image (C) was transformed into a refractive index contour. Finally, the droplet's boundary layer thickness was measured at the

center position of each droplet, and the vapor area was measured. However, a window was selected and fixed at the highest point of the droplet in the beginning, which means that the decrease in the droplet's height was neglected in our study.

4. RESULTS AND DISCUSSIONS

4.1 Relation between Knife-edge Position and Light Intensity

According to the calculation processes performed in our study, the relation between the knife-edge position and the intensity needs to be confirmed at first. A single image was taken at different knife-edge positions away from the reference position in the vertical direction. The reference position was fixed at a 100% cut-off position. The intensity value was measured by averaging all the image pixels' intensities present in each image. Figure 6 clearly confirms that the knife-edge position has a linear relation with the light intensity, and the assumption used in the calculation is valid. The result shows that at 100% cut-off, there was no light passing through the knife edge resulting in no intensity being sensed by the camera. Furthermore, the intensity value linearly increased when the knife edge moved away from the reference position.

4.2 Droplet's Lifetime (t_e)

Lifetimes of single and double droplets are shown in Figure 7. The result clearly shows that the higher ethanol concentration case has a shorter droplet lifetime than that for the lower ethanol concentration case since ethanol is more volatile than water. This agrees with the result reported by Sefiane et al. [27], Shi et al. [30], and Cheng et al. [31]. In addition, although Gurralla et al. [32] performed the experiment with a heated substrate, their results at a 25 $^{\circ}$ C substrate temperature can be compared with our results, where the ambient temperature is close to their substrate temperature. The results show good agreement with each other in terms of a faster evaporation rate with increasing volatile matter composition. Moreover, it was found that the double droplet case has a longer lifetime than that of the single droplet case at all concentration values. In this study, the average evaporation rate of the droplet was separated into the average total evaporation rate and the average evaporation rate per droplet as shown in Table II. The average total evaporation rate of the double droplet was found to be higher than that of the single droplet. On the other hand, the evaporation rate per droplet of the

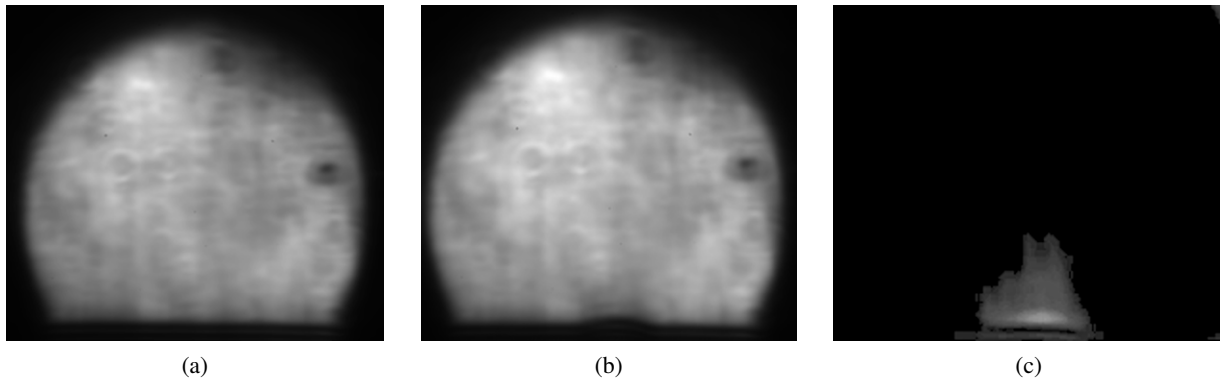


Figure 5. (a) Reference image (A), (b) Schlieren image (B), and (c) pure evaporation image (C).

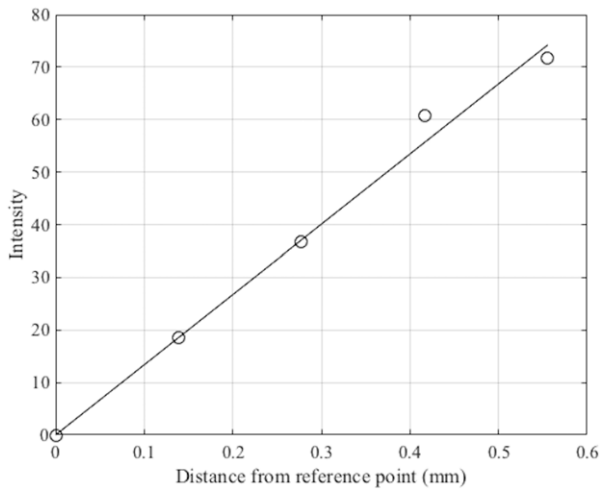


Figure 6. Linear relation between knife-edge position and intensity.

double droplet was found to be smaller than that of the single droplet. Referring to Eq. (2) provided by Kobayashi et al. [24], since L was approximately equal to $2R$ in our study, the average evaporation rate per droplet of the double droplet case should be $2/3$ of the single droplet evaporation rate. The largest gap in the total droplet's lifetime between single and double droplets was found in the pure water case, in which the double droplet evaporation rate per droplet was approximately $3/4$ of that of the single droplet. This value is very close to the prediction from Eq. (2). However, the difference in terms of droplets' lifetimes between single and double droplets decreased as the concentration of ethanol increased, and they were found to be very close in high ethanol concentration cases. The trend is different from the prediction from Eq. (2). The difference between our results and the prediction from Eq. (2) provided by Kobayashi et al. [24] is due to the difference in the substance. Equation (2) was based on a pure water substance and our experiments were conducted using ethanol–water mixtures. With ethanol–water mixtures, not only the evaporation of ethanol but also the evaporation and condensation of water should be considered, and this makes the problem more complicated. In addition, the difference may be due

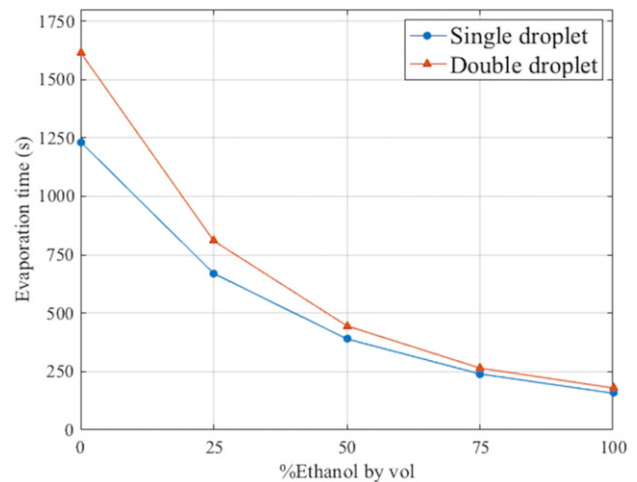


Figure 7. Droplet's lifetime (t_e) at each ethanol concentration of single and double droplet cases.

to the effect of the relative humidity difference in each experiment since the experiments were conducted at a wide range of relative humidity values. More experiments and considerations are needed in the future.

4.3 Thickness of Boundary Layer of Droplet

All results were obtained from the experiments and fitted by a second-order polynomial. However, in the following results, the decrease in droplet height was neglected as mentioned in Section 3.3. The boundary layer thicknesses of single and double droplets as functions of normalized time (t/t_e) are illustrated in Figures 8(a) and 8(b), respectively. In both cases, a thicker boundary layer was found as the ethanol concentration was increased. For the single droplet, an increase in the thickness of the boundary layer in the beginning was found for a high concentration of ethanol: 75% ethanol concentration and pure ethanol. This is due to the diffusion of ethanol vapor into the air. After reaching the highest point, it started to drop due to both gravity and evaporation of the droplet since ethanol is heavier than air. In contrast, a linear decreasing trend of the thickness of the boundary layer value was found for a low concentration of ethanol. Nonetheless, both trends were found for the

Table II. Comparison between total average evaporation rate and average evaporation rate per droplet of pure water.

Case	Initial volume Total/per droplet (μL)	Lifetime (s)	Average total evaporation rate ($\mu\text{L/s}$)	Average evaporation rate per droplet ($\mu\text{L/s}$)
Single droplet	2.5/2.5	1233	0.0020	0.0020
Double droplet	5.0/2.5	1616	0.0031	0.0015

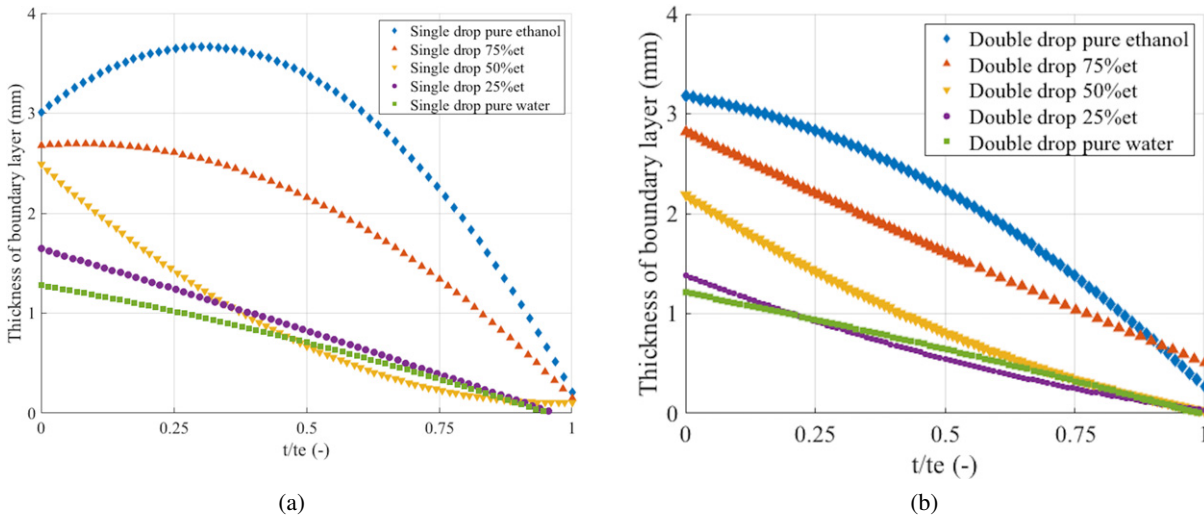


Figure 8. The thickness of boundary layer with normalized time (t/t_e) for pure substances and three different mixtures of (a) single droplet and (b) double droplet.

50% case, which drastically decreased in the beginning and gradually dropped at the end. The results agreed with those of Sefiane et al. [27] and Shi et al. [30] that high ethanol concentration (75%) exhibited a behavior similar to that of pure ethanol while the behavior at low concentration (25%) was similar to that of pure water. However, a small difference was detected in the case of the double droplet. The behavior of 75% ethanol concentration of the double droplet case was similar to that of the ethanol concentration of 50% rather than that of pure ethanol.

To compare single and double droplets' boundary layer thicknesses, Figures 9(a) and 9(b) show their comparison at high and low concentrations of ethanol, respectively. A thicker boundary layer was found for the single droplet at all concentrations. Moreover, the increase in boundary layer thickness in the beginning for high ethanol concentration (75%) and pure ethanol cases was not observed in the double droplet case, which was in contrast to the single droplet case. This may be due to the larger gravity effect occurring in the double droplet case. The more the ethanol vapor, the larger the gravity effect that was expected. Schlieren images used to compare single and double droplets are illustrated in Figures 10(a) and 10(b), respectively. On the other hand, a similar trend and value between single and double droplets were found in the low ethanol concentration case (25%) and pure water.

4.4 Effect of Boundary Layer Thickness

The thickness of the boundary layer presented in Eq. (1) has an effect on the evaporation rate of the droplet, in particular when the value is small. The time changes of the relative thickness can be defined as in the following equation:

$$\text{relative thickness} = \frac{l}{R}, \quad (10)$$

where l is the instantaneous thickness of the boundary layer of the droplet and R is the instantaneous radius of the droplet.

Figure 11 shows the relative thickness of the pure substance. The results show that the thickness of the boundary layer is of the same order as that of the droplet radius, and it cannot be neglected in estimating the evaporation rate. However, in the presented experimental results, the thickness of the boundary layer and the vapor area obtained from the Schlieren system are considered as qualitative measurement regarding the sensitivity of the system. The relation between the evaporation rate estimated from the results of the Schlieren approach and that from the observation and the prediction accuracy will be reported in detail in the next paper.

4.5 Vapor Area of Droplet

The vapor area was defined by the region of the vapor that formed over the droplet. The value was measured from the vapor region detected in the pure evaporation image

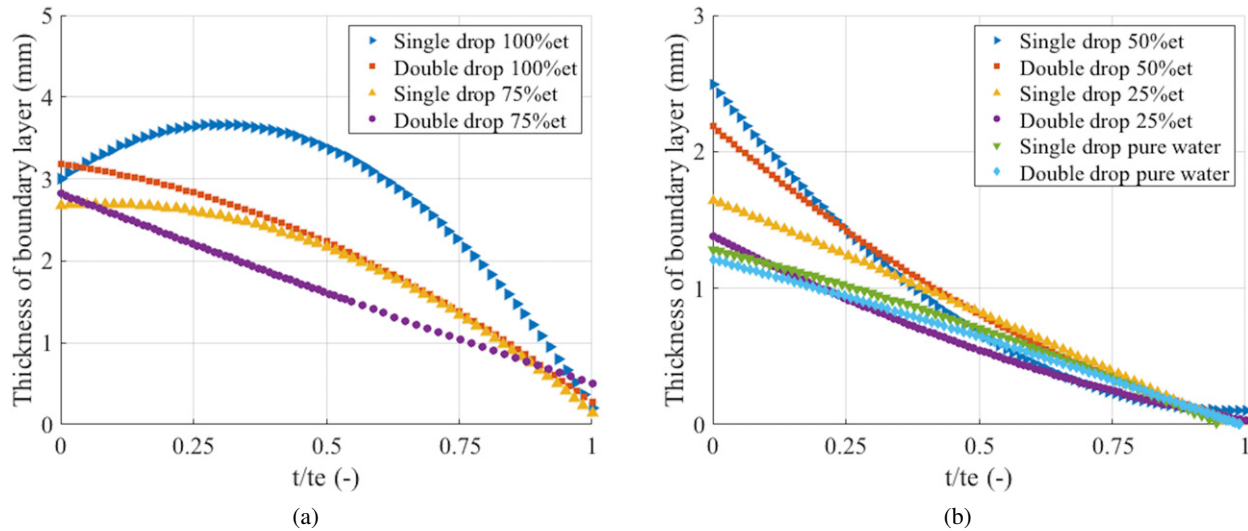


Figure 9. Comparison of boundary layer thicknesses for single and double droplet cases at (a) high ethanol concentrations and (b) low ethanol concentrations.

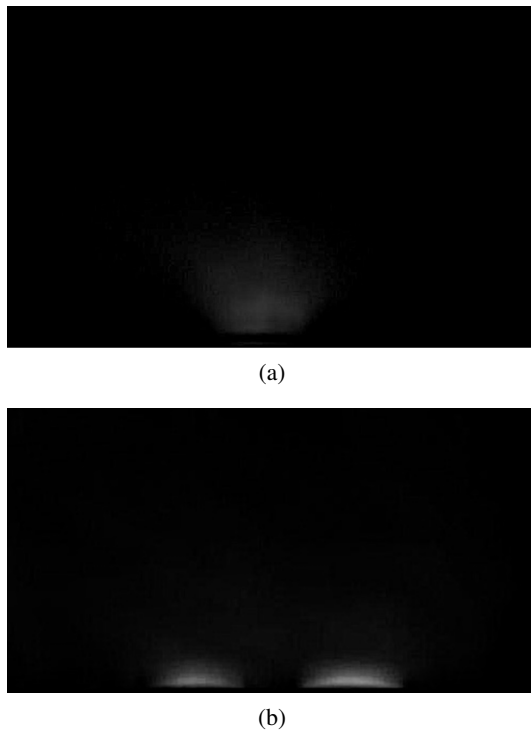


Figure 10. Schlieren images of pure ethanol at $t/t_e = 0.25$ of (a) single droplet and (b) double droplet.

as mentioned in Section 3.3. In the case of the double droplet, it represents the total region of vapor evaporated from both droplets. First, by comparing this to the droplet's lifetime, it is indicated that a larger vapor area means a higher total instantaneous evaporation rate since a decrease in the vapor area was found as the ethanol concentration is decreased in both single and double droplets. Figures 12(a) and 12(b) show that a similar trend for the boundary layer thickness can be identified between high ethanol concentration (75%) and pure ethanol and also between low ethanol concentration (25%) and pure water. Moreover,

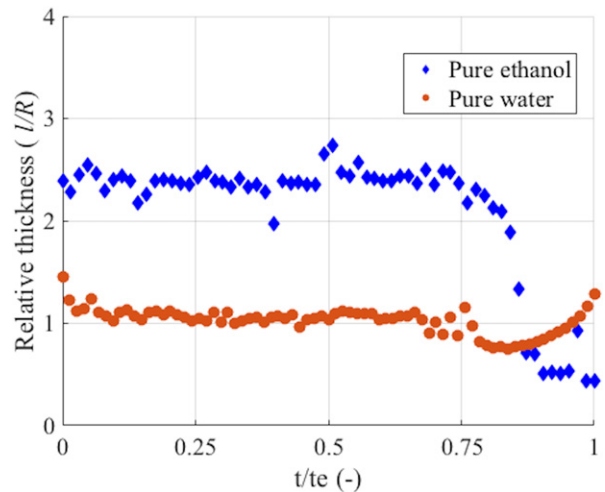


Figure 11. Relative thickness for pure substances with normalized time (t/t_e).

the 50% ethanol concentration case represented a high concentration trend in the beginning and low concentration at the end, which is similar to the result for the boundary layer thickness.

However, an opposite trend from the boundary layer thickness was observed by comparing single and double droplets. The double droplet case had a larger total vapor area than that of the single droplet at all ethanol concentrations as shown in Figures 13(a) and 13(b). In summary, the thickness of the boundary layer and the vapor area compared between single droplet and double droplet cases showed an inverse relation: a thicker boundary layer was found in the single droplet case and a larger total vapor area was found in the double droplet case.

Figure 14 illustrates the relation for the normalized vapor area, which is defined as the fraction between the vapor area of the double droplet and the single droplet as in the

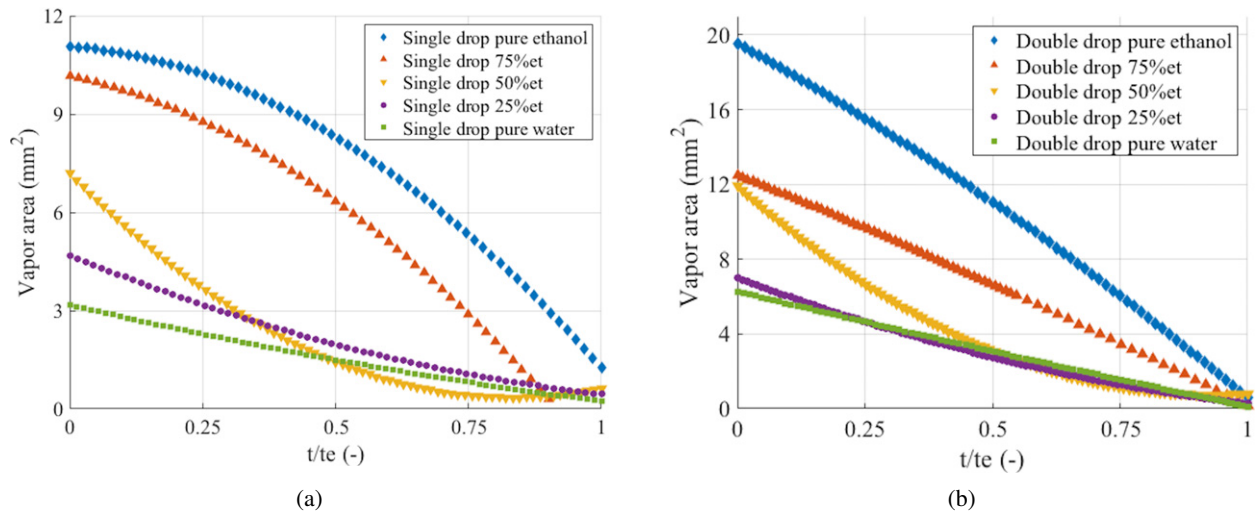


Figure 12. Vapor area with normalized time (t/t_e) for pure substances and three different mixtures of (a) single droplet and (b) double droplet.

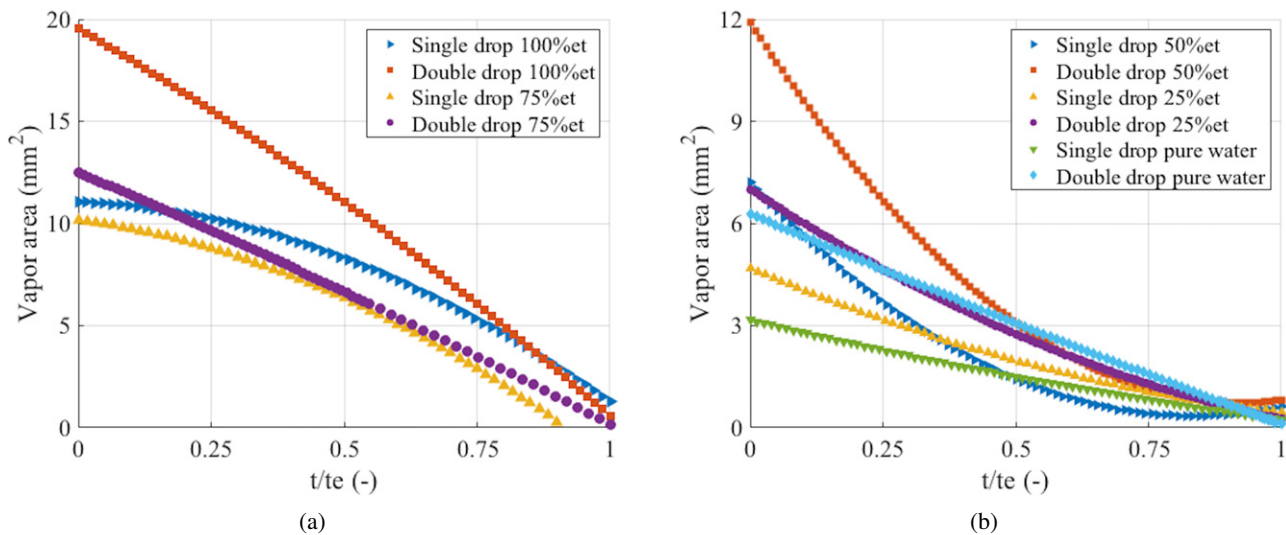


Figure 13. Comparison of vapor areas for single and double droplet cases at (a) high ethanol concentrations and (b) low ethanol concentrations.

following equation:

$$\text{normalized area} = \frac{A_{dd}}{A_{sd}}, \quad (11)$$

where A_{dd} is the double droplet's vapor area and A_{sd} is the single droplet's vapor area.

The result shows that the total instantaneous vapor region of the double droplet was larger than that of the single droplet similarly to the case where the average total evaporation rate of the double droplet was higher than that of the single droplet as mentioned in Section 4.2. However, the relations among the evaporation rate, the boundary layer thickness, and the area of vapor are complicated, and more experiments and considerations are needed in future work.

5. CONCLUSIONS

Our work presents an experimental measurement of a droplet's boundary layer thickness and investigation of the

effect of a neighboring droplet on the evaporation rate by means of the Z-type Schlieren technique. Ethanol-water mixtures at concentrations of 75%, 50%, and 25% together with pure ethanol and water were selected instead of water-based ink because the sensitivity of the Schlieren system depends on the refractive index and water vapor's refractive index is very close to the surrounding air, causing difficulty in extracting the vapor region. The significant results from our study can be concluded as follows:

1. An increase in ethanol concentration decreased the droplet's lifetime in both single and double droplets, which agreed with the previous studies [27, 30, 31] and recently reported results of Gurralla et al. [32]. The average evaporation rate per droplet of the double droplet was approximately 3/4 of that of the single droplet in the pure water case, which was consistent with the result of Kobayashi [24]. However, the lifetimes of single and double droplets were found to be very

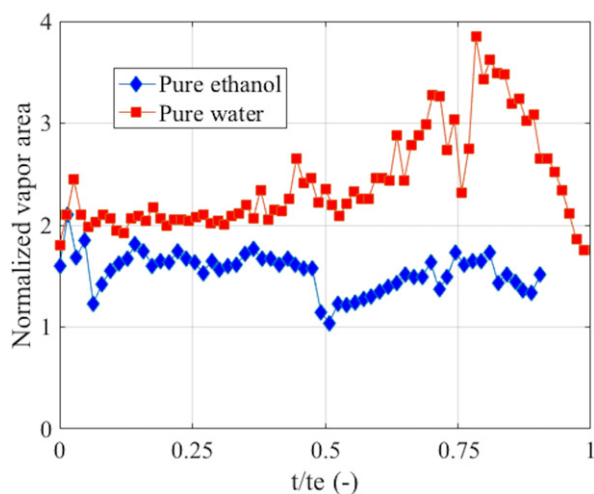


Figure 14. Normalized vapor area (A_{dd}/A_{sd}) with normalized time of pure substance.

close in the high ethanol concentration case, which was in contrast to the model of Kobayashi [24]. This is due to the difference in the substance used—pure water in Kobayashi [24] and ethanol–water mixtures in our study—and may be due to the difference in relative humidity in each experiment, which needs to be thoroughly investigated in a future study.

- An increase in the boundary layer thickness due to diffusion was observed in the beginning of high ethanol concentration in the single droplet case while this was not found in the double droplet case. In the single droplet case, the result clearly showed that high ethanol concentration followed a similar trend to pure ethanol whereas low ethanol concentration followed the behavior of pure water. This agreed with the studies of Sefiane et al. [27] and Shi et al. [30]. However, a small difference was observed in the double droplet case. High ethanol concentration's behavior was similar to that of 50% ethanol concentration rather than that of pure ethanol. By comparing single and double droplet cases, it was found that the single droplet had a thicker boundary layer than that of the double droplet at all ethanol concentrations. This might be because the effect of gravity on the double droplet was larger than that on the single droplet.
- By defining the relative thickness, the results show that the thickness of the boundary layer cannot be neglected for estimating the evaporation rate since it has the same order as the radius of the droplet. However, since the Schlieren system provided qualitative measurement regarding the sensitivity of the system, the relation between results obtained from the Schlieren system and the evaporation rate as well as the accuracy of the system itself should be considered in future investigation.
- A larger vapor area was found for higher ethanol concentration. A high ethanol concentration also followed the behavior of pure ethanol, and low ethanol concentration followed the behavior of pure water, which is the same result as that for the boundary layer thickness. However,

an opposite result was found for the boundary layer thickness. The area of the double droplet was larger than that of the single droplet in all cases.

- By defining and calculating the normalized vapor area, it was found that the total instantaneous vapor area for the double droplet case was found to be larger than that for the single droplet case. In contrast, the average evaporation rate per droplet in the single droplet case was found to be higher. However, a relation between the instantaneous vapor area and the instantaneous evaporation rate has not been clearly reported in this study. This will be studied and discussed in a future study.

6. FUTURE PROSPECTS

As mentioned earlier, our experiments were conducted for a wide range of relative humidity ratios. Hence, we expect to perform experiments for a narrower range. Furthermore, in the next step, we plan to compare the evaporation rate of the droplet calculated from our measured boundary layer thickness with the equations provided by other studies. Finally, since the results were related to the system sensitivity, their relation should be explored in the future study as well.

ACKNOWLEDGMENTS

The authors acknowledge the technical support and fruitful discussion with Mr. Motoi Koda, former technician at Tokyo Institute of Technology. They also appreciate the help from Dr. Haruo Iimura, researcher from Ricoh Company, Ltd.

REFERENCES

- P. Calvert, "Inkjet Printing for Materials and Devices," *Chem. Mater.* **13**, 3299 (2001).
- B.-J. de Gans, P. C. Duineveld, and U. S. Schubert, "Inkjet printing of polymers: State of the art and future developments," *Adv. Mater.* **16**, 203 (2004).
- B.-J. de Gans and U. S. Schubert, "Inkjet printing of well-defined polymer dots and arrays," *Langmuir* **20**, 7789 (2004).
- M. Ikegawa and H. Azuma, "Droplet behaviors on substrates in thin-film formation using ink-jet printing," *JSM E Int. J. B* **47**, 490 (2004).
- J. Park and J. Moon, "Control of Colloidal Particle Deposit Patterns within Picoliter Droplets Ejected by Ink-Jet Printing," *Langmuir* **22**, 3506 (2006).
- D. Kim, S. Jeong, B. K. Park, and J. Moon, "Direct writing of silver conductive patterns: Improvement of film morphology and conductance by controlling solvent compositions," *Appl. Phys. Lett.* **89**, 264101 (2006).
- D. P. Siregar, J. G. M. Kuerten, and C. W. M. van der Geld, "Numerical simulation of the drying of inkjet-printed droplets," *J. Colloid Interface Sci.* **392**, 388 (2013).
- M. Kimura, M. J. Misner, T. Xu, S. H. Kim, and T. P. Russell, "Long-range ordering of diblock copolymers induced by droplet pinning," *Langmuir* **19**, 9910 (2003).
- H. Komiyama, D. Hojo, K. Z. Suzuki, S. Mizukami, T. Adschiri, and H. Yabu, "Binary nanoparticles coassembly in bioinspired block copolymer films: a stepwise synthesis approach using multifunctional catechol groups and magneto-optical properties," *ACS Appl. Nano Mater.* **1**, 1666 (2018).
- M. Chopra, L. Li, H. Hu, M. A. Burns, and R. G. Larson, "DNA molecular configurations in an evaporating droplet near a glass surface," *J. Rheology* **47**, 1111 (2003).
- T. P. Bigioni, X.-M. Lin, T. T. Nguyen, E. I. Corwin, T. A. Witten, and H. M. Jaeger, "Kinetically driven self assembly of highly ordered nanoparticle monolayers," *Nature Mater* **5**, 265 (2006).

- 12 R. Bhardwaj, X. Fang, and D. Attinger, "Pattern formation during the evaporation of a colloidal nanoliter drop: a numerical and experimental study," *New J Physics* **11**, 11 (2009).
- 13 H. Nakao, S. Tokonami, T. Hamada, H. Shiigi, T. Nagaoka, F. Iwata, and Y. Takeda, "Direct observation of one-dimensional plasmon coupling in metallic nanofibers prepared by evaporation-induced self-assembly with DNA," *Nanoscale* **4**, 6814 (2012).
- 14 N. N. Lebedev, "Special functions and their applications," *Physics Today* **18**, 70 (1965); translated to English by Richard A. Silverman.
- 15 R. G. Picknett and R. Bexon, "The evaporation of sessile or pendant drops in still air," *J. Colloid Interface Sci.* **61**, 336 (1977).
- 16 K. S. Birdi, D. T. Vu, and A. Winter, "A study of the evaporation rates of small water drops placed on a solid surface," *J. Phys. Chem.* **93**, 3702 (1989).
- 17 R. D. Deegan, O. Bakajin, T. F. Dupont, G. Huber, S. R. Nagel, and T. A. Witten, "Capillary flow as the cause of ring stains from dried liquid drops," *Nature* **389**, 827 (1997).
- 18 R. D. Deegan, O. Bakajin, T. F. Dupont, G. Huber, S. R. Nagel, and T. A. Witten, "Contact line deposits in an evaporating drop," *Phys. Rev. E* **62**, 756 (2000).
- 19 H. Hu and R. G. Larson, "Evaporation of a sessile droplet on a substrate," *J. Phys. Chem. B* **106**, 1334 (2002).
- 20 S. Semenov, A. Trybala, R. G. Rubio, N. Kovalchuk, V. Starov, and M. G. Velarded, "Simultaneous spreading and evaporation: recent developments," *Adv. Colloid Interface Sci.* **206**, 382 (2014).
- 21 F. Girard, M. Antoni, and K. Sefiane, "Infrared thermography investigation of an evaporating sessile water droplet on heated substrates," *Langmuir* **26**, 4576 (2010).
- 22 G. Fabien, M. Antoni, and K. Sefiane, "Use of IR thermography to investigate heated droplet evaporation and contact line dynamics," *Langmuir* **27**, 6744 (2011).
- 23 T. Yamaue, "Measurement and simulation of a drying droplet on a substrate," *J. Japan Soc. Colour Material* **81**, 504 (2008) [In Japanese].
- 24 M. Kobayashi, M. Makino, T. Okuzono, and M. Doi, "Interference effects in the drying of polymer droplets on substrate," *J. Phys. Soc. Japan* **79**, 044802 (2010).
- 25 M. Doi, "Physics of evaporation and drying—evaporation induced flow and structural formation," *Butsuri* **73**, 551 (2018) [In Japanese].
- 26 P. L. Kelly-Zion, C. J. Pursell, R. S. Booth, and A. N. VanTilburg, "Evaporation rates of pure hydrocarbon liquids under the influences of natural convection and diffusion," *Int. J. Heat Mass Transfer* **52**, 3305 (2009).
- 27 K. Sefiane, L. Tadrast, and M. Douglasa, "Experimental study of evaporating water–ethanol mixture sessile drop: influence of concentration," *Int. J. Heat Mass Transfer* **46**, 4527 (2003).
- 28 J. R. E. Christy, Y. Hamamoto, and K. Sefiane, "Flow transition within an evaporating binary mixture sessile drop," *Phys. Rev. Lett.* **106**, 20570 (2011).
- 29 C. Liu, E. Bonaccorso, and H. J. Butta, "Evaporation of sessile water/ethanol drops in a controlled environment," *Phys. Chem. Chem. Phys.* **10**, 7150 (2008).
- 30 L. Shi, P. Shen, D. Zhang, Q. Lin, and Q. Jiang, "Wetting and evaporation behaviors of water–ethanol sessile drops on PTFE surfaces," *Surf. Interface Anal.* **41**, 951 (2009).
- 31 A. K. H. Cheng, D. M. Soolaman, and H.-Z. Yu, "Evaporation of micro-droplets of ethanol–water mixtures on gold surfaces modified with self-assembled monolayers," *J. Phys. Chem. B* **110**, 11267 (2006).
- 32 P. Gurrara, P. Katre, S. Balusamy, S. Banerjee, and K. C. Sahu, "Evaporation of ethanol-water sessile droplet of different compositions at an elevated substrate temperature," *Int. J. Heat Mass Transf.* **145**, 118770 (2019).
- 33 P. Katre, P. Gurrara, S. Balusam, S. Banerjee, and K. C. Sahu, "Evaporation of sessile ethanol-water droplets on a highly inclined heated surface," Preprint arXiv:2003.09628.
- 34 G. S. Settles, *Schlieren and Shadowgraph Techniques* (Springer, New York, 2001), pp. 25–74.
- 35 G. S. Settles and M. Hargather, "A review of recent developments in schlieren and shadowgraph techniques," *Measurement Sci. Technol.* **28**, 042001 (2017).
- 36 C. A. Herrera, D. M. Hernandez, B. B. Garcia, and J. A. Guerrero-Viramontes, "Temperature measurement of air convection using a Schlieren system," *Opt. Laser Technol.* **41**, 233 (2009).